

HEALTH AND MEDICINE

A facile one-stage treatment of critical bone defects using a calcium sulfate/hydroxyapatite biomaterial providing spatiotemporal delivery of bone morphogenetic protein–2 and zoledronic acid

Deepak Bushan Raina^{1*}, Lucas-Maximilian Matuszewski², Corina Vater², Julia Bolte², Hanna Isaksson^{1,3}, Lars Lidgren¹, Magnus Tägil¹, Stefan Zwillingenberger²

Bone morphogenetic proteins (BMPs) are the only true osteoinductive molecules. Despite being tremendously potent, their clinical use has been limited for reasons including supraphysiological doses, suboptimal delivery systems, and the pro-osteoclast effect of BMPs. Efforts to achieve spatially controlled bone formation using BMPs are being made. We demonstrate that a carrier consisting of a powder of calcium sulfate/hydroxyapatite (CaS/HA) mixed with bone active molecules provides an efficient drug delivery platform for critical femoral defect healing in rats. The bone-active molecules were composed of osteoinductive rhBMP-2 and the bisphosphonate, and zoledronic acid (ZA) was chosen to overcome BMP-2–induced bone resorption. It was demonstrated that delivery of rhBMP-2 was necessary for critical defect healing and restoration of mechanical properties, but codelivery of BMP-2 and ZA led to denser and stronger fracture calluses. Together, the CaS/HA biomaterial with rhBMP-2 and/or ZA can potentially be used as an off-the-shelf alternative to autograft bone.

INTRODUCTION

A critical-sized bone defect is defined as the minimum-sized bone defect, which will not “spontaneously” heal unless other interventions are applied (1). High-energy fractures or recalcitrant fractures can lead to substantial bone loss and critical bone defects (2). These defects require mechanical stability and additional healing stimuli as part of the treatment regime. Mechanical stability is achieved using internal, external, or intramedullary fixation hardware (2), while healing stimuli emanate from a bone-grafting material such as autografts. Autologous bone is the “gold standard” in orthopedic surgery as it provides (i) a scaffold for bone regeneration, (ii) a rich source of progenitor cells, and (iii) the necessary biomolecules such as bone morphogenetic proteins (BMPs) to heal the defect (3). Despite being appealing, shortcomings including donor-site morbidity, risk of infection, and lack of adequate graft volume have led to an increased demand for an off-the-shelf substitute to the autologous bone (4). On the surgical front, a promising surgical technique for healing of critical defects in humans, without the use of exogenous BMPs, is the induced membrane or the Masquelet technique, which involves a two-stage procedure (5). The technique has shown excellent results in the treatment of large bone defects (6) but is still limited by autograft availability, making the development of an off-the-shelf bone substitute a necessity. Furthermore, use of a two-stage procedure causes patient morbidity and increased costs to the health care system.

Biomaterial researchers are constantly trying to develop the “magic” material to potentially replace autologous bone graft with benefits of unlimited supply. Biomaterials mimicking the bone struc-

ture physicochemically have evolved as promising alternatives (7) to autografts, but functionalizing biomaterials with bone active molecules in large bone defects in bone tissue engineering is a sine qua non due to the lack of inherent bone-inducing cytokines. One of the most promising bone active molecules is the Food and Drug Administration (FDA)–approved BMP-2 (rhBMP-2), the only approved bioactive molecule for healing of bone defects available in the market. Spatiotemporal delivery of the protein during the bone healing phase is mandatory (8) but not achieved with the currently provided carrier, an absorbable collagen sponge (ACS) (9). Among other reasons, BMPs are hesitantly used by orthopedic surgeons due to the supraphysiological clinical doses applied (10) since the carrier does not provide controlled delivery of the protein. Our group has experimentally shown that BMPs, in addition to bone formation, also accelerate premature bone resorption as seen by large but empty calluses, inferior from a bone mechanics perspective (11). The phenomenon of excessive bone resorption can be experimentally counteracted using bisphosphonates, such as zoledronic acid (ZA), administered either locally or systemically (12, 13). ZA induces apoptosis of the osteoclasts within a fracture callus and counteracts the high resorptive drive induced via the RANKL (receptor activator of nuclear factor kappa-B ligand)–RANK (receptor activator of nuclear factor kappa-B) system due to BMP usage (14). This has been shown to aid in achieving a net-positive bone turnover, stronger fracture calluses, and with reduced rhBMP-2 doses (11, 15). We recently demonstrated that a clinically approved calcium sulfate/hydroxyapatite (CaS/HA) biomaterial provides controlled and long-term delivery of both rhBMP-2 and ZA in an ectopic extraosseous muscle pouch model (16). The CaS/HA biomaterial used in this study was developed at the orthopedic biomaterials laboratory at the Lund University and is approved for human use by the regulatory authorities both in Europe and North America. The material is clinically used for filling bone voids (17, 18) and for the local delivery of antibiotics in the treatment of debrided osteomyelitis (19, 20). CaS/HA provides

Copyright © 2020
The Authors, some
rights reserved;
exclusive licensee
American Association
for the Advancement
of Science. No claim to
original U.S. Government
Works. Distributed
under a Creative
Commons Attribution
NonCommercial
License 4.0 (CC BY-NC).

¹Lund University, Faculty of Medicine, Department of Clinical Sciences Lund, Orthopaedics, Lund 22185, Sweden. ²University Hospital Carl Gustav Carus at Technische Universität Dresden, University Center of Orthopedic, Trauma and Plastic Surgery, Dresden 01307, Germany. ³Lund University, Department of Biomedical Engineering, Lund 22100, Sweden.

*Corresponding author. Email: deepak.raina@med.lu.se

a simple platform to be used in surgery and consists of a premixed powder of 60 weight % (wt %) CaS and 40 wt % HA, which sets into a hard mass in situ in approximately 15 min when mixed with saline and/or nonionic radiographic agents. In 2016, our group described the possibility of using this biomaterial as a carrier for rhBMP-2 and ZA in vivo in the muscle pouch model (13) and later in a tibia defect model (21). On the basis of our earlier findings, we envisaged to use the CaS/HA carrier for healing of a critical-sized bone defect in rats. HA is a key component of the bone known to chemically interact with both rhBMP-2 (22) and ZA (23).

An important goal of translational research strategies is the feasibility of the proposed approach. Several carriers have been proposed for the delivery of bone active molecules for critical defect healing. A majority of them often involve tedious fabrication strategies, and the preparation in the operating room remains a challenge due to practical reasons (24). The goal of this study was to use a clinically tested CaS/HA biomaterial that could provide an easy-to-implement single-stage platform for the delivery of the bone active molecules such as rhBMP-2 and ZA in a clinically relevant critical bone defect model in rats. On the basis of the existing results from earlier studies, we hypothesized that the CaS/HA biomaterial will provide spatio-temporal delivery of both rhBMP-2 and ZA, at least during the first 4 weeks of defect healing (16). Furthermore, it was hypothesized that the biomaterial will provide a congenial matrix for bone ingrowth considering its favorable in vivo resorption rate (25).

RESULTS

A 5-mm critical mid-diaphyseal defect in Wistar rats of 10 to 12 weeks of age was created (see fig. S1 for surgical procedure), and the defect was augmented with a CaS/HA biomaterial with or without bioactive molecules, BMP-2 and ZA. The defect healing was evaluated at 6 and 12 weeks after surgery. The schematic of the study, timelines, and evaluation techniques are shown in Fig. 1 and Table 1.

One specimen from the CaS/HA + ZA group and CaS/HA + rhBMP-2 + ZA had to be excluded from all analysis at 12 weeks due to infection and failure to remove the fixation plate around the defect, respectively. Two specimens from CaS/HA + rhBMP-2 + ZA groups (one defect and one contralateral) had to be removed from the three-point bending analysis due to technical issues during testing.

Radiographic consolidation at 6 weeks

At 6 weeks, CaS/HA + rhBMP-2 (G4) and CaS/HA + rhBMP-2 + ZA (G5) groups demonstrated 83 and 100% bridging, respectively (Fig. 2A), while no bridging was seen in groups G1 to G3 (Fig. 2A shows representative x-ray images, while fig. S2 shows all specimens).

Defect consolidation at 12 weeks: Radiography and micro-computed tomography

No bridging was seen in the empty controls (G1), CaS/HA (G2), or CaS/HA + ZA (G3) groups (Fig. 2B). The defects in CaS/HA + rhBMP-2 (G4) and CaS/HA + rhBMP-2 + ZA (G5) groups demonstrated 83 and 91% bridging, respectively at 12 weeks. The results from ex vivo x-ray analysis at 12 weeks are shown in Fig. 2B (see fig. S3 for images of all specimens).

In the treated legs, the bone volume (BV) within the defect was significantly higher in both CaS/HA + rhBMP-2 (G4) group and in the CaS/HA + rhBMP-2 + ZA (G5) group when compared to CaS/HA (G2) alone or CaS/HA + ZA (G3) (Fig. 3, A and B).

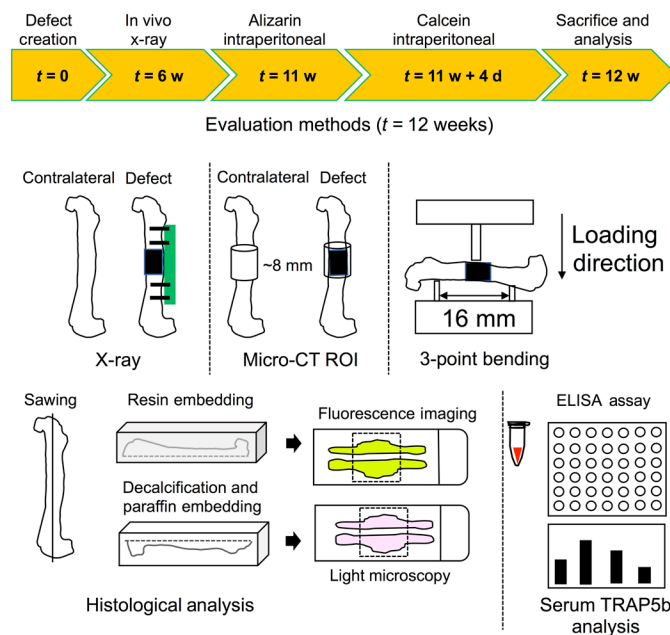


Fig. 1. Overview of the timeline and the evaluation techniques used in the evaluation of defect healing in the rat critical femoral defect model. An interim analysis of bone healing was performed using in vivo x-ray radiography at 6 weeks, followed by ex vivo analysis of bone healing at the terminal time point of 12 weeks using x-rays for evaluating radiographic union and using micro-computed tomography (micro-CT) for quantification of new bone volume (BV) and bone mineral density. Mechanical properties of regenerated bone were studied using three-point bending. Some of the intact femurs were also studied histologically. Resin-embedded bone specimens were used to study late mineral apposition, while paraffin histology was performed to study the type of regenerated bone [using hematoxylin and eosin (H&E) staining and Goldner's trichrome staining] and distribution of blood vessels in the regenerated bone tissue (using α -smooth muscle actin staining). A detailed description of sample size used for each evaluation technique is provided in Table 1. ROI, region of interest; ELISA, enzyme-linked immunosorbent assay; TRAP5b, tartrate-resistant acid phosphatase 5b.

The BV in CaS/HA + rhBMP-2 + ZA (G5) was also significantly higher than CaS/HA + rhBMP-2 (G4). No differences in the BV of the contralateral legs in the four treatment groups were observed (fig. S4A). Furthermore, no differences in the bone mineral density of the treated or the contralateral legs were seen (Fig. 3C and fig. S4B).

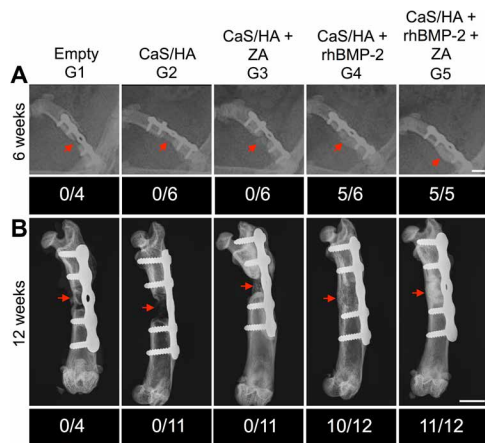
Comparison of BV of the defect and the contralateral leg within each treatment group revealed an increased defect BV only in CaS/HA + rhBMP-2 (G4) and CaS/HA + rhBMP-2 + ZA group (G5) (Fig. 3, D and E). The other two groups either had a lower BV in the defect leg compared to the contralateral leg (CaS/HA; fig. S4C) or the BV remained unchanged (CaS/HA + ZA) as shown in fig. S4D. Bone mineral density in the contralateral leg was significantly higher compared with the defect legs in all treatment groups as shown in fig. S5 (A to D).

Restoration of bone biomechanical properties

Only CaS/HA + rhBMP-2 (G4) and CaS/HA + rhBMP-2 + ZA (G5) groups fit the inclusion criteria (defect bridging) for the three-point bending test. The peak force to fracture the defect leg in the CaS/HA + rhBMP-2 + ZA (G5) group was significantly higher than that in the CaS/HA + rhBMP-2 group (G4) (209.1 N, 173.6 to 244.5 versus 147.6 N, 96.8 to 198.4; $P < 0.05$; Fig. 4A).

Table 1. Study overview including treatment groups, doses, evaluation methods, and sample size. Overview of the study with treatment, doses, and sample sizes used for each evaluation method. Indicated doses of bioactive molecules are dose per animal. *n* indicates sample number/treatment.

Treatment	Sample size total (<i>n</i>)	X-ray 6 weeks (<i>n</i>)	X-ray 12 weeks (<i>n</i>)	Micro-CT 12 weeks (<i>n</i>)	3-point bending 12 weeks (<i>n</i>)	Histology 12 weeks (<i>n</i>)	TRAP5b 12 weeks (<i>n</i>)
G1. Empty	4	4	4	3	0	3	3
G2. CaS/HA	11	6	11	11	0	4	9
G3. CaS/HA + ZA (10 μg)	11	6	11	10	0	4	10
G4. CaS/HA + rhBMP-2 (15 μg)	12	6	12	12	8	4	10
G5. CaS/HA + rhBMP-2 (15 μg) + ZA (10 μg)	12	5	11	11	7	4	10

**Fig. 2. Representative radiological images from groups G1 to G5 at 6 and 12 weeks after surgery.** (A) In vivo radiological assessment at 6 weeks after surgery on living animals. (B) Ex vivo radiological assessment of explanted femora at 12 weeks after surgery. The arrows point at the defect. The number below each image represents the number of samples that showed radiographic bridging in each treatment group. Scale bars, ~5 mm.

No differences in the peak force, stiffness, or absorbed energy were seen in the contralateral legs of both treatment groups (fig. S6, A to C). No differences in the peak force, stiffness, or absorbed energy of the defect versus the contralateral legs could be observed in both CaS/HA + rhBMP-2 (fig. S7, A to C) and CaS/HA + rhBMP-2 + ZA (fig. S7, D to F) groups, indicating complete restoration of mechanical properties of the bone.

To ascertain that the three-point bending results represented the mechanical properties of the fracture callus and not the native bone, we recorded the location of each fracture as shown in Fig. 4D. Irrespective of the treatment groups, all fractures in the defect legs occurred through the callus, while a mixed response of transverse, oblique, and spiral fractures was seen in the contralateral legs (Fig. 4E).

Microscopic assessment of bone healing

Bone mineral deposition

To study the late mineral apposition in different treatment groups, we used fluorochromes alizarin red and calcein. Fluorescent imag-

ing of the defect regions in the empty (G1), CaS/HA (G2), and CaS/HA + ZA (G3) groups revealed two distinct bands of red (alizarin) and green (calcein) at the extreme end of the cortical defect both proximally and distally, indicating ongoing mineral deposition (Fig. 5). High-magnification imaging of the defect center revealed no signal, indicating no further mineralization.

The neocortex of the rhBMP-2 (G4)- and rhBMP-2 + ZA (G5)-treated groups exhibited relatively weaker bands of red and green, indicating that the process of mineralization in the cortical bone might have reached its end. However, some periosteal remodeling could still be observed. In the two rhBMP-2-treated groups (G4 and G5), mineral deposition was more homogeneous and also visible in the defect regions, while in the other groups, it was only concentrated at the bony ends.

Histological assessment of healing grades and blood vessel formation

Goldner's trichrome and hematoxylin and eosin (H&E)-stained images indicated a visible defect gap in the empty (G1), CaS/HA (G2), and CaS/HA + ZA (G3) groups, which was filled primarily with fibrous tissue (Fig. 6A). High-magnification H&E-stained images of CaS/HA (G2) and CaS/HA + ZA (G3) groups also showed remnants of the biomaterial within the defect. CaS/HA + rhBMP-2 (G4) and CaS/HA + rhBMP-2 + ZA (G5) groups indicated fully restored neocortex (Fig. 6A). These groups also demonstrated the presence of the cancellous bone within the defect and that the trabecular islands were filled either with CaS/HA remnants or with bone marrow-like tissue. CaS/HA remnants were also seen in other parts of the defect, indicating partial resorption of the material at the 12-week time point. Material degradation appeared to be in synergy with the rate of bone ingrowth characterized by the presence of lesser CaS/HA biomaterial remnants in both rhBMP-2-treated groups, consolidating that the material does not hinder bone ingrowth. When comparing G4 and G5, the cortical bone was thinner in G4, and the defect center was filled with more bone marrow-like tissue and empty spaces when compared to G5. In G5, potentially because of the presence of ZA, CaS/HA remnants were more prominent. In both G4 and G5, the neocortex were composed mostly of the lamellar bone, while a mix of lamellar and woven bone structures could be observed in the middle of the defect. Huo *et al.* (26) classification system corroborated the micro-computed tomography (micro-CT) and gross microscopic results. CaS/HA + rhBMP-2 (G4) and CaS/HA +

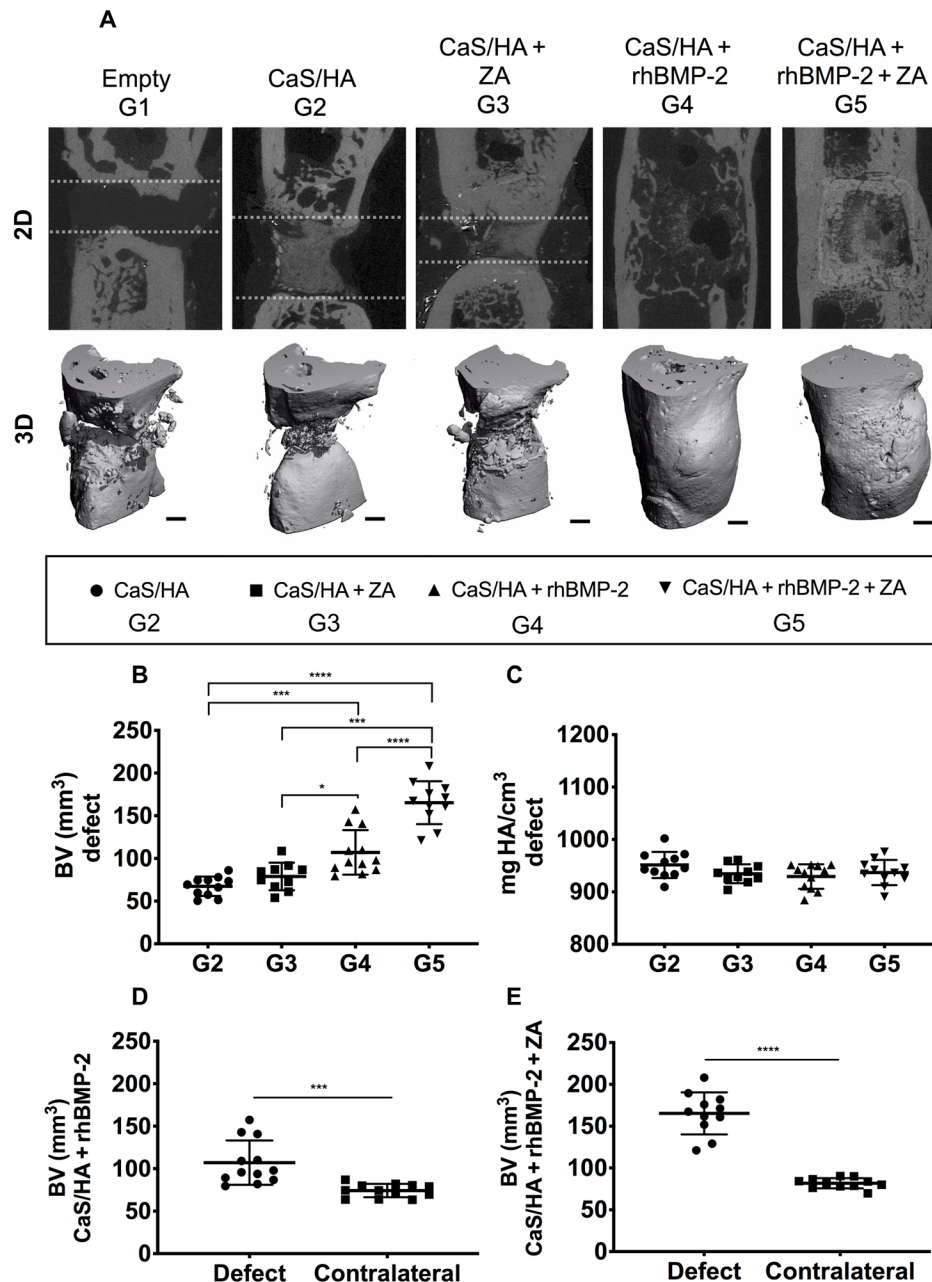


Fig. 3. Micro-CT–based evaluation of critical defect healing 12 weeks after surgery in groups G1 to G5. (A) Representative two-dimensional (2D) slices (top) and 3D reconstructions (bottom), (B) BV, and (C) density/BV quantified in the defect area in all treatment groups using micro-CT. (D and E) Comparison of the BV measured in the defect versus contralateral legs of animals treated with CaS/HA + rhBMP-2 and CaS/HA + rhBMP-2 + ZA, respectively. White dashed lines in (A) represents defect gap at 12 weeks. Data are presented as means \pm SD. * P < 0.05, *** P < 0.001, and **** P < 0.0001. Additional micro-CT data are provided in figs. 4 and 5. Scale bars, 1 mm.

rhBMP-2 + ZA (G5) demonstrated an average histological grade of defect healing of 9.5, which corresponds to complete defect bridging with a mixture of mature and immature bone (Fig. 6B).

α -Smooth muscle actin (α SMA) staining revealed that the specimens in the empty (G1), CaS/HA (G2), and CaS/HA + ZA (G3) groups were predominantly filled with fibrous tissue in the defect center and contained more blood vessels in the defect area, while the cortical bone was sparsely vascularized (Fig. 7, A and B). Blood vessels were also seen in close proximity to the CaS/HA biomaterial. In the groups that exhibited complete bridging, i.e., CaS/HA + rhBMP-2

and CaS/HA + rhBMP-2 + ZA, the neocortex had only a few blood vessels and similar findings applied to the defect center where only a few α SMA-positive blood vessels were visible, especially in the intratrabecular spacing, which was filled with bone marrow–like tissue (Fig. 7B).

Local bisphosphonate treatment does not hinder bone remodeling

The serum level of tartrate-resistant acid phosphatase 5b (TRAP5b) was significantly higher in the CaS/HA + ZA (3.6 U/liter, 2.8 to 4.5;

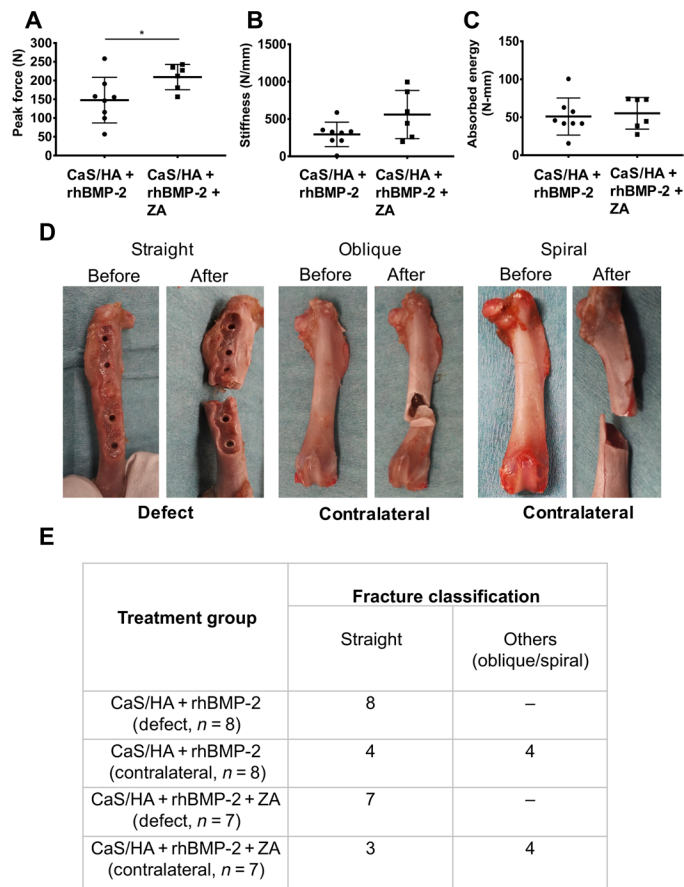


Fig. 4. Three-point bending of the explanted femora 12 weeks after surgery to assess the biomechanical properties of the regenerated bone in G4 and G5. (A) Peak force to fracture, (B) stiffness, and (C) absorbed energy measured in the defect leg of the two groups. (D) Representative images emphasizing the type of fracture occurring in the defect and contralateral legs. Notice the straight transverse fracture in the defect leg in all specimens (D and E) and a mix of transverse, oblique, and spiral fractures on the contralateral leg (D and E). Data are presented as means ± SD. **P* < 0.05. Photo credit: Deepak Bushan Raina, Lund University.

P < 0.05) and CaS/HA + rhBMP-2 + ZA (4.4 U/liter, 3.8 to 4.9; *P* < 0.001) groups when compared to CaS/HA control (2.1 U/liter, 1.4 to 2.8; Fig. 6C). No differences between only CaS/HA + rhBMP-2 and other treatment groups were observed.

DISCUSSION

The aim of this study was to establish a simple, one-step surgical intervention to enable healing of a critical femoral defect in rats, which eventually could be translated clinically. This was achieved using a CaS/HA-based bone substitute as a carrier for the controlled delivery of FDA-approved bioactive drugs. The ability of biomaterials in regenerating large volumes of the bone is limited and hinders their clinical translation. This is why the delivery of osteoinductive rhBMP-2 was hypothesized to be necessary (27). Further, local codelivery of ZA would aid in hindering the pro-osteoclastic effects of rhBMP-2 (12). At the end of 6 and 12 weeks, the results of this study indicated that radiographic union could only be achieved in groups where rhBMP-2 was delivered. Further, at 12 weeks, the combined delivery of rhBMP-2 + ZA not only led to complete bridging but also led to

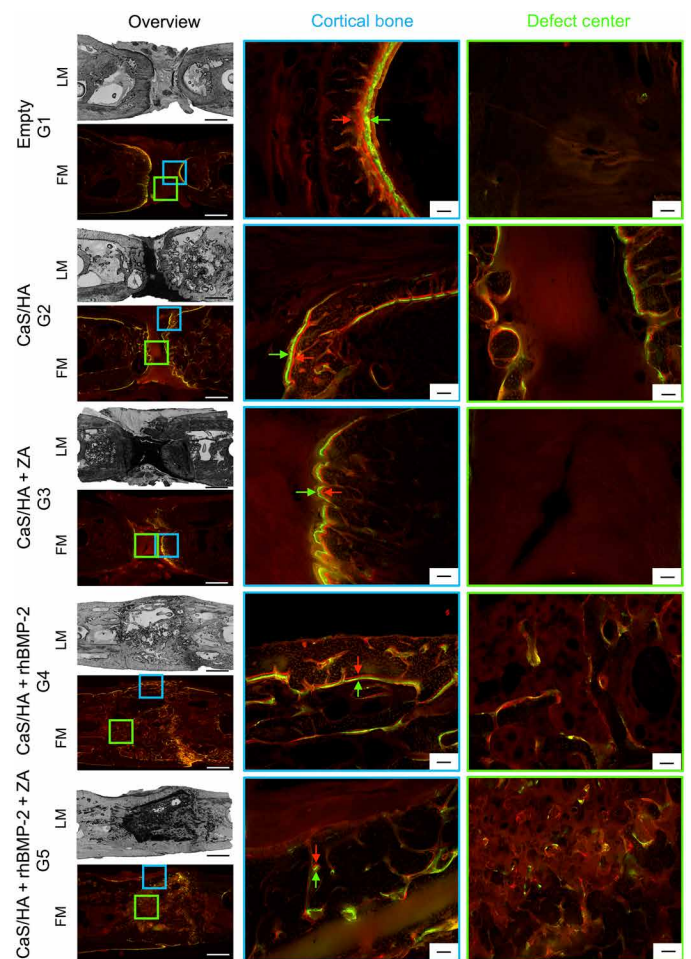


Fig. 5. Representative histological images of the defect from groups G1 to G5 analyzed under fluorescent light. Red (alizarin, injected 7 days before euthanasia) and green (calcein, injected 3 days before euthanasia) bands indicate mineral apposition fronts, which can be seen between the green (calcein) and red (alizarin red) arrows. LM, light micrograph; FM, fluorescent image. Scale bars (overview images) 1.5 mm, (magnified images of the cortical bone and the defect center) 100 micrometer.

the production of a denser and stronger callus compared to rhBMP-2 delivery alone as seen from micro-CT, mechanical testing, and histology. Thus, the hypothesis that codelivery of rhBMP-2 + ZA would aid in complete bridging of the defect and would lead to stronger fracture callus was verified.

In light of the results of this study, it is important to emphasize that achieving spatiotemporal release of both rhBMP-2 and ZA from the CaS/HA biomaterial was an important prerequisite for critical defect healing. The in vivo release kinetics of rhBMP-2 and ZA from the CaS/HA biomaterial has been well characterized, and the existing data showed that after a 4-week implantation period, the biomaterial releases 60% rhBMP-2 and 20% ZA (16), which is superior to the release kinetics of rhBMP-2 achieved from the current FDA-approved ACS for rhBMP-2 delivery (9). Codelivery of rhBMP-2 in the presence of ZA does not have any effect on the biological activity or release profile of rhBMP-2 (28). In a preceding study, our group carried out a head-to-head comparison of the CaS/HA-based biomaterial with the ACS biomaterial in an ectopic muscle pouch model in rats (15).

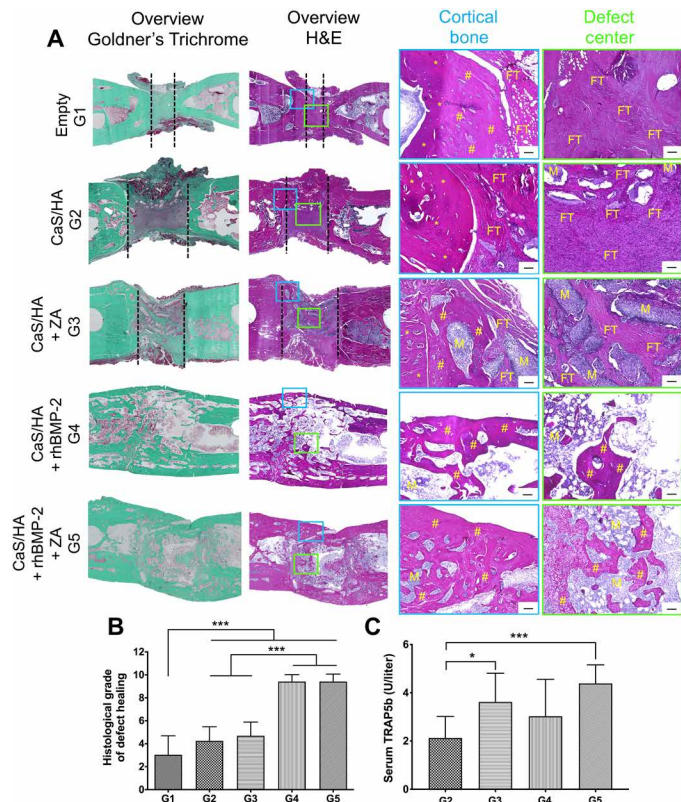


Fig. 6. Representative histological images of the defect legs in groups G1 to G5 stained with Goldner's trichrome and H&E and quantification of serum TRAP5b levels as a surrogate marker of bone remodeling. Black dashed lines in (A) indicate the region where the defect is not bridged. In trichrome-stained images, green color indicates bone, and purple/red shows fibrous tissue, muscle, or bone marrow. In H&E images, asterisks (*) indicate old cortical bone, number signs (#) indicate new bone, FT indicates fibrous tissue, and M indicates remnants of the CaS/HA biomaterial. (B) Fracture healing score according to Huo *et al.* (26) where a score of 1 represents fibrous tissue in the defect and score of 10 indicates bony union filled with the mature bone. (C) Levels of osteoclast biomarker TRAP5b measured in the serum of all animals at the 12-week time point using ELISA. Data are presented as means \pm SD. *** $P < 0.001$. Scale bars, 100 μ m.

The aim of the study was to compare the ability of both the carriers in delivering rhBMP-2 and the eventual bone formation in a challenging experimental model. It was elucidated that the rhBMP-2 release kinetics and net bone formation are tightly coupled and the CaS/HA-based scaffold led to significantly higher bone formation than the ACS biomaterial when same doses of rhBMP-2 (10 μ g) were delivered from both the biomaterials. It is also noteworthy to mention that the ACS biomaterial is a poor carrier of ZA due to the lack of a ZA-binding domain in the ACS biomaterial (such as HA) as shown by Murphy and co-workers (29), thus making it less efficient for codelivery of both rhBMP-2 and ZA (15). The major CaS component of the CaS/HA biomaterial resorbs within a period of 6 weeks (25), implying that the release of rhBMP-2 is coupled with the rate of degradation of the biomaterial. However, ZA strongly binds to HA and does not show a similar release pattern (16). Loosely bound ZA embedded in the CaS/HA biomaterial is released within a month, while the remaining ZA stays bound to HA. This is an advantage in a fracture healing scenario. rhBMP-2 is known to prematurely resorb the bridging callus (11), which may lead to decreased

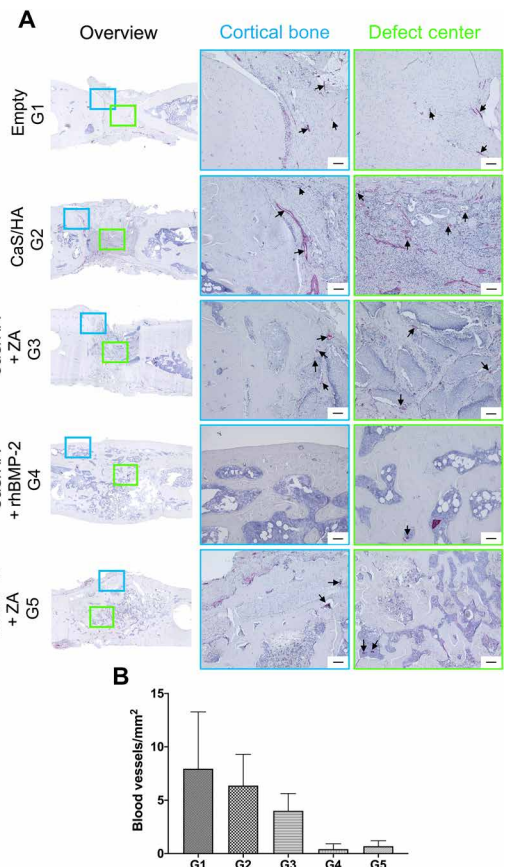


Fig. 7. Representative immunohistochemical staining of the blood vessels (using α SMA as a marker) in the defect legs in groups G1 to G5 groups analyzed under a light microscope. (A) Arrows point to α SMA-positive cells and blood vessels (red color). (B) Data from the quantification of blood vessels per square millimeter in each treatment group. Data are presented as means \pm SD. Scale bars, 100 μ m.

strength and, by speculation, a reason for the clinical shortcoming and limited use in patients. Availability of ZA locally, at the site of the bone formation, can aid in preventing this event as elucidated by the micro-CT and biomechanical testing results in this study.

This is the first experimental study describing the use of CaS/HA biomaterial in combination with BMP-2 and ZA for treatment of a critical-sized defect. Several critical defect models have been described in rats recapitulating intramembranous and endochondral ossification. In the rat femur, a defect size of >4 mm is considered to be critical (30), meaning that it will not heal without an external intervention in the form of surgery and defect augmentation. The rat femoral defect model is a well-accepted and clinically relevant model of bone formation as the healing undergoes endochondral ossification and large defect volumes can be achieved to create a challenging environment for bone regeneration (31, 32). The radiological follow-up 12 weeks after operation of the small set of animals ($n = 4$) belonging to the empty group indicated no bridging in any of the specimens, consolidating the critical size of the defect used in this study.

The FDA-approved dosage of rhBMP-2 delivered via the ACS is 1.5 mg/cm³ (33). The volume of a CaS/HA cylinder used to fill the defect in this study was approximately 0.063 cm³ per defect, indicating a dose reduction of approximately six times compared to the

maximum recommended dose for orthopedic trauma in humans when normalized by scaffold volume [maximum recommended dose normalized to scaffold volume (94.5 μg) versus rhBMP-2 dose used in study (15 μg)]. No abnormal bone cysts were observed in the bone defect as reported earlier in the literature when rhBMP-2 with >22.5 μg of doses was used (34). In addition, it is important to mention that the dose of rhBMP-2 used in this study did not lead to heterotopic ossification, a common side effect of supraphysiological rhBMP-2 dose delivered clinically (10). Krishnan *et al.* (35) showed that delivery of 30 μg of rhBMP-2 in a rat femur defect model using either the ACS material or a self-developed alginate-based delivery system led to ectopic bone formation around the defect. It remains unknown whether this is a problem associated with the carrier per se, which deforms and leaks into the surrounding tissue, or if supraphysiological doses are responsible for this phenomenon. According to a recent study, the heterotopic ossification is more likely to be related to the carrier, and efficient sequestration of high-dose BMP-2 in heparin microspheres did significantly reduce ectopic bone formation (31). Apart from high rhBMP-2 doses and uncontrolled spatiotemporal release of rhBMP-2, another potential cause of heterotrophic bone formation around the implanted carrier could be the mechanical properties of the carrier. Collagen sponges do not have sufficient mechanical properties per se and undergo deformation in wet state (15) contrary to the CaS/HA biomaterial, which allows for filling of complex geometries before setting into a hard mass. Segredo-Morales and co-workers (24) reviewed studies using BMP-2 delivery for treatment of femoral defects and indicated a dose range of 1 to 50 μg for treatment of critical femoral defects in rats experimentally. Either the studies conducted with low-dose (1 μg) rhBMP-2 reported radiographic bridging only, without any qualitative analysis of the functional properties of the regenerated bone such as bone mechanics (36), or results showed no difference in the biomechanical properties (35).

In this study, three-point bending was chosen over torsional testing. As reported in a previous study from our group comparing a torsion testing setup with a three-point bending setup, the fracture callus in BMP + ZA-treated animals was stiffer than the native bone. This led to breaking of the femur proximal or distal to the fracture, in parts of the intact femur weaker than regenerated callus (37), and, therefore, did not reflect the biomechanical properties of the regenerated bone. In this study, all specimens from the defect leg fractured through the callus, thus representing the true mechanical characteristics of newly regenerated bone/material composite. Another noteworthy observation to discuss is that in the rhBMP-2 and rhBMP-2 + ZA groups, the peak force to fracture in the defect legs was similar to the contralateral leg, indicating complete restoration of the mechanical properties. From these results, one could also conclude that by codelivery of rhBMP-2 + ZA via the CaS/HA biomaterial, it might be possible to further lower the rhBMP-2 doses and still achieve full restoration of biomechanical properties of the bone at the same time.

We surveyed the literature to find the lowest effective dose of a growth factor used to heal a critical femoral defect in rats. A recent study by Zhang *et al.* (32) indicated a dose of 0.4 μg of BMP-2/7 heterodimer per animal to heal a 5-mm critical defect in rats. Direct comparison of homodimer BMP-2 and heterodimer BMP-2/7 doses is not possible, but studies have shown the heterodimer to be significantly more potent than the homodimers of BMP-2 and BMP-7 alone (38). Further studies are warranted for clinical use of the heterodimer BMP-2/7 as inflammatory responses have been indicated

to be a reason of concern with BMPs in general (10). Further, the heterodimer protein is not approved by the FDA for clinical use.

ZA is a potent bisphosphonate, which is administered systemically to retard the excessive bone resorption in osteoporosis. In experimental studies, systemic treatment of ZA has been combined with local BMP delivery to achieve dense and strong fracture unions (11, 12), but the treatment with systemic ZA comes with its own downsides such as myalgia/flu-like symptoms, reduced overall bone remodeling, atypical cortical bone fractures (39), and less common osteonecrosis of the jaw with prolonged usage in patients given ZA the first time (40, 41). Circumventing these side effects while maintaining the antiosteoclast effect could be relevant clinically. Local use of ZA, particularly around implants, has shown promising results with increased bone-implant anchorage (16). Our group also demonstrated that locally delivered ZA in a rat tibia defect model had a profound effect on the cancellous bone regeneration, but rather unexpectedly, it did not enhance cortical bone healing (42). The ZA group in this study did not demonstrate any effect on the critical defect healing either. Keeping these findings in mind, one can conclude that the cortical and cancellous compartments of the bone not only are structurally different but also involve different healing stimuli. Usage of local ZA could be criticized since it alters the physiological bone remodeling process, especially at the high doses achieved by local delivery. To test this hypothesis, we also evaluated serum TRAP5b levels, an osteoclast-specific biomarker in all animals (43). Rather unexpectedly, the results indicated elevated TRAP5b activity in both the ZA-treated groups (G3 and G5) compared to CaS/HA control group. This could imply that the physiological bone remodeling is not impaired with local ZA delivery at the doses used in this study. This emphasizes the importance of using a biphasic material for codelivery of both rhBMP-2 and ZA. ZA released from the fast-resorbing CaS phase prevents early bone resorption, but once released, the remaining ZA bound to the HA phase does not affect further remodeling. However, it is imperative to perform a longitudinal assessment of serum TRAP5b as the levels of TRAP5b in the CaS/HA + rhBMP-2 group after 12 weeks had returned to baseline. This could mean that the BMP-2-induced osteoclastogenesis and elevated TRAP5b levels might be detected at earlier time points such as at 6 weeks.

We believe that there are a few open questions that we could not address in the current study. Because of the large number of study groups, we were restricted to have only one complete follow-up of bone healing using all evaluation techniques, although radiographic evaluation indicated healing in rhBMP-2 and rhBMP-2 + ZA groups already after 6 weeks. It is difficult to speculate whether the biomechanical properties of the bone also were restored at that early time point. Nevertheless, we can conclude that codelivery of rhBMP-2 and ZA is superior to delivering rhBMP-2 alone. To speculate whether this combination also could accelerate, the critical defect healing would require an early time point. Using the current study setup, we could not elucidate the source of cells responsible for healing of the critical defect, and more sophisticated tissue isolation techniques and lineage tracking studies would be required. Last, a future aim would be to find out the lowest effective dose of rhBMP-2 required to heal the defect. In this study, we chose a dose range high enough to promote bone healing and simultaneously avoid side effects such as ectopic ossification. Further studies are warranted to establish the minimum effective rhBMP-2 dosage and additional larger animal studies warranted before clinical translation.

In this study, a critical-sized femoral defect model in rats was used to investigate a CaS/HA-based biomaterial functionalized with bioactive molecules rhBMP-2 and ZA alone or in combination to obtain controlled delivery of drugs enhancing bone regeneration. With a defect size of 5 mm, the model was critical, and the specimens in the empty, CaS/HA, and CaS/HA + ZA groups did not heal. After 6 weeks, the defects in the BMP-2 and BMP-2 + ZA groups already bridged radiographically, and almost 100% defect bridging was seen in these two groups at the terminal time point of 12 weeks. The use of ZA, together with rhBMP-2, made the fracture calluses stronger and denser, and the restoration of mechanical properties of the defect leg was achieved in both groups. All measurements were verified by histological analysis, which showed viable bone even in the center of the defect. We demonstrate that a synthetic biomaterial combined with rhBMP-2 and ZA can be used as an off-the-shelf alternative to the autologous bone in critical bone defects in rats. Since all ingredients are approved for clinical use, the combination may replace or even supersede the effect of conventional bone grafting techniques in the near future. This would facilitate surgery for nonunion and critical defects to a large extent.

MATERIALS AND METHODS

Preparation of CaS/HA biomaterial

The CaS/HA biomaterial (provided by the manufacturer BONESUPPORT AB, Sweden) was prepared by mixing CaS/HA with iohexol, an iodine-based radiographic contrast agent, at a liquid-to-powder ratio of 0.43 ml/g of CaS/HA powder. A total of four different formulations of the CaS/HA biomaterial were prepared, which were based on the experimental groups. The first type consisted of pure CaS/HA, and the biomaterial was prepared by mixing 500 mg of CaS/HA powder with 215 μ l of liquid (62.5 μ l of saline + 152.5 μ l of contrast agent) in a well of a sterile 48-well plate. After thorough mixing for 1 min, the slurry was transferred into a 1-ml syringe using a spatula and extruded into four cylindrical wells of a silicone mold ($\varnothing = 4$ mm and $h = 6$ mm). Each well was fully filled, and the material was allowed to set for 30 min before recovering it by cutting the silicone mold using blades. Because of surface tension, the material concaved at the top, thereby producing a cylinder of approximately 5 mm in height and 4 mm in diameter. This process was repeated another two times to achieve a total of 12 cylindrical grafts. The second variant of the CaS/HA biomaterial contained ZA (Novartis, Switzerland; original concentration, 0.8 mg/ml reconstituted in saline). Same steps as described above were followed except that the mixing solution contained 62.5 μ l of ZA solution (50 μ g) and 152.5 μ l of contrast agent. This liquid was mixed to 500 mg of CaS/HA powder to obtain four cylindrical grafts of CaS/HA + ZA biomaterial containing 10 μ g of ZA per cylinder. The process was repeated two more times to obtain 12 cylindrical grafts. The third composition consisted of the CaS/HA biomaterial containing rhBMP-2 (part of a InductOs bone graft kit, Medtronic, Dublin, Ireland). A total of 75 μ g of BMP-2 was mixed with 62.5 μ l of saline and 152.5 μ l of contrast agent to form the BMP solution (concentration, 0.35 mg/ml), which was mixed with 500 mg of CaS/HA powder to achieve four cylinders of CaS/HA + rhBMP-2 biomaterial containing 15 μ g of rhBMP-2 per graft. Cylinders were casted in the same way as described above, and the process was repeated until 12 scaffolds were achieved. Last, the last composition of the CaS/HA biomaterial was composed of CaS/HA + rhBMP-2 + ZA. A total of 75 μ g of BMP-2 was mixed

with 62.5 μ l of ZA (concentration, 0.8 mg/ml) and 152.5 μ l of contrast agent to form the BMP + ZA solution (concentration, 0.35 mg/ml), which was mixed with 500 mg of CaS/HA powder to achieve four cylinders of CaS/HA + rhBMP-2 + ZA biomaterial containing 10 μ g of ZA + 15 μ g of rhBMP-2 per graft. CaS/HA slurry for approximately one graft volume was always wasted partly during transferring the contents into the syringe and partly in the syringe used for extrusion, explaining why ZA and rhBMP-2 were calculated for five grafts in each mixing procedure. Preparation of the biomaterial scaffolds was performed under sterile conditions in a laminar airflow bench, and the grafts were implanted within 48 hours of casting the biomaterial.

Critical defect model and surgery

Ten- to 12-week-old male Wistar rats (weight, 398 ± 25 g; range, 356 to 480 g) were purchased from JANVIER LABS (France). The rats were anesthetized using a mixture of isoflurane (3%) and O₂ maintained at a flow rate of 2 liter/min. Then, animals were placed in prone position on a 37°C warm heating pad, isoflurane was lowered to 2 to 2.5%, which was maintained during the entire duration of the surgery, and buprenorphine (Temgesic, 30 μ g/kg; Indivior Europe Ltd., Dublin, Ireland) was injected subcutaneously for analgesia. The right hind limb of the animal was shaved and disinfected, and an approximately 3-cm-long skin and fascia incision was made along the length of the right femur [fig. S1, A and B (i)].

Another 2-cm incision was made between the musculus tensor fasciae latae femoris and the musculus vastus lateralis to expose the deeper muscle layers. Blunt separation of the musculus rectus femoris and the musculus vastus lateralis was performed using spatulas (fig. S1B, ii), and the femur was exposed (fig. S1B, iii). After thoroughly cleaning the femur laterally from soft tissue, a customized five-hole internal fixation plate (\varnothing of 1.5-mm straight locking plate, stainless steel; LCP Compact Hand System, DePuy Synthes, Warsaw, USA) was applied to the lateral aspect of the femur and held in place using forceps and a clamp. At this point, the plate was permanently fixed to the bone using two proximal and two distal screws (\varnothing of 1.5-mm locking screws, stainless steel; outer screws, 7 mm in length; inner screws, 6 mm in length; DePuy Synthes). Screw holes were created in the femur using drill sleeves and a 1.1-mm \varnothing drill bit (DePuy Synthes). A custom-made, three-dimensional (3D) printed saw guide (fig. S1C, i) was then placed on the lateral femur above the third empty hole of the plate, and a 5-mm osteotomy was performed using two Gigli wires (0.44 mm; RISystem AG, Landquart, Switzerland). The piece of mid-diaphyseal bone was carefully removed (fig. S1C, ii), and the wound was thoroughly rinsed with saline to remove metallic remnants of the Gigli wires. A defect of approximately 5 mm was achieved in all animals, which was calculated by measuring the length of the removed piece of bone (means \pm SD, 4.55 ± 0.3 mm; range, 4.0 to 5.4 mm) and the thickness of the Gigli wire. The defect was then treated as follows: (G1) empty, (G2) CaS/HA, (G3) CaS/HA + ZA, (G4) CaS/HA + rhBMP-2, and (G5) CaS/HA + rhBMP-2 + ZA (see Table 1 for sample size). The cylindrical grafts were push-fitted and not secured with any sutures (fig. S1C, iii and iv). In some cases, the implant was scraped at one end using a scalpel to ensure good fitting into the defect. The wound was closed in a layered fashion using resorbable sutures (Vicryl 4-0, Ethicon, Somerville, USA) by closing the muscle first (continuous interlaced suture), followed by closing the skin (Donati suture). After wound closure, animals were transferred back into their cage and allowed to wake up under

an infrared lamp. Animals started load bearing immediately after surgery.

Some animals from each group were subjected to *in vivo* x-ray analysis 6 weeks after operation, whereas all animals received two different fluorescent fluorochromes 1 week before euthanizing (Fig. 1). All animals were euthanized 12 weeks after operation. Anesthesia was induced by isoflurane inhalation (3%), followed by blood sampling from each animal collected via the intracardiac route. Anesthetized animals were then euthanized by CO₂ asphyxiation, and both femora (defect and contralateral) were harvested before being subjected to x-ray, micro-CT, three-point bending, and histology. An overview of the timelines and evaluation techniques is also provided in Fig. 1, and a detailed description of the experimental groups and number of specimens used for each evaluation technique is provided in Table 1.

In vivo x-ray radiography at 6 weeks

At 6 weeks after surgery, randomly selected animals ($n = 4$ to 6 per group; Table 1) were anesthetized using isoflurane (3%) and placed in a right lateral decubitus position. Both hind limbs were secured to the bottom x-ray plate using adhesive tape before obtaining a lower body x-ray using a movable x-ray device (AMX 4 Plus, GE Medical Systems, Chicago, USA) with an x-ray tube voltage of 50 kV and 1-mA-s electric charge. X-rays were judged to be bridged or not bridged by two orthopedic surgeons. A specimen was judged to be bridged if complete cortical healing along the length of the defect was observed.

Ex vivo x-ray radiography and micro-CT at 12 weeks

Harvested, native femora from each animal were placed in pairs and imaged using a microradiography device (MX-20, Faxitron, Tucson, USA) with 30-kV operating voltage and an exposure time of 5 s. After acquiring the x-ray, the internal fixation plate was carefully removed from each specimen to void disturbing the tissue formed in the defect. Each sample was then wrapped with cling film, individually placed in a test tube and imaged in a micro-CT instrument (vivaCT 40, Scanco Medical, Wangen-Brüttisellen, Switzerland) with an isotropic voxel size of 21 μm . The most proximal and distal screw holes were used to define the micro-CT scanning area, which corresponded to a volume of interest of approximately 11 mm (525 slices). After the scans were completed, samples were randomly divided for either three-point bending or histological analysis. Histology specimens were fixed in neutral buffered formalin (4%), while the specimens for three-point bending were frozen at -80°C until the day before testing. Micro-CT image sets from each sample were analyzed using the SCANCO Medical software suite. An approximately 8-mm (380 slices, starting from the end of the proximal drill hole nearest to the defect to the beginning of the distal drill hole nearest to the defect) cylindrical region of interest (ROI) was defined to quantify the bone regenerated in the defect. The same was performed for the nontreated contralateral legs, and the mid-diaphysis was chosen as the ROI. After calibration according to manufacturer's protocols, a threshold of 400 mg of HA/cm³ was used to identify the bone and was kept constant for all specimens. BV and tissue mineral density (density/BV) were used as the two outcome variables of the micro-CT assessment.

Biomechanical testing

Samples that either exhibited complete or partial bridging were chosen for mechanical testing. One day before the three-point bending tests, samples were thawed at 4°C overnight before bringing them to

room temperature 1 hour prior testing. The samples were then placed on a custom-made three-point bending jig consisting of a bottom holder with two brass indenters that are 16 mm apart (Fig. 1). Digital images of all specimens were captured. The top indenter was connected to the 15-kN sensor of the Instron load frame (8511 biaxial model, High Wycombe, U.K) operated by MTS Flex Test 40 Controller (MTS TestSuite Multipurpose Elite Software, MTS, Eden Prairie, USA). An automated algorithm was defined on the controller program, which allowed to load the samples at a rate of 1 mm/s until fracture. After failure, all specimens were photographed again and analyzed by three independent observers to classify and document the fracture into three categories: (i) straight, (ii) oblique, or (iii) spiral.

Histological assessment of critical defect healing

After the micro-CT imaging, four treated femora from each group were randomly selected for histological examination. Each bone was cut along the sagittal plane and perpendicular to the screw holes in two almost equal halves. As seen in Fig. 1, one half was embedded in Technovit 9100 (Kulzer GmbH, Wehrheim, Germany) and used for fluorescent analysis, whereas the other one was decalcified with EDTA, embedded in paraffin (Engelbrecht, Edermünde, Germany), and used for (immuno-)histological staining.

Fluorescent staining for mineral apposition

To assess bone formation and remodeling *in vivo*, animals received two fluorescent calcium-binding dyes 1 week before euthanizing. The first fluorophore, alizarin (2 wt % in 2 wt % NaHCO₃, 20 mg/kg; Fluka, Honeywell, Morristown, USA), was injected 7 days before euthanasia, and the second fluorophore, calcein (2 wt % in 2 wt % NaHCO₃, 20 mg/kg; Fluka), was injected 3 days before euthanasia of the animals. Both fluorophores were injected intraperitoneally. All animals were euthanized at the 12-week time point, femora were explanted, cut, embedded in Technovit 9100, grinded to a thickness of 50 to 100 μm , and imaged using a Keyence BIOREVO BZ-9000 microscope (Keyence, Osaka, Japan; alizarin: tetramethyl rhodamine isothiocyanate filter, excitation: 545/25, emission: 605/70; calcein: green fluorescent protein filter, excitation: 470/40, emission: 525/50).

Goldner's trichrome and H&E staining

Decalcified, paraffin-embedded, specimens were cut to a thickness of 2.5 μm and stained with Goldner's trichrome and H&E (Merck, Darmstadt, Germany) using standard procedures and digitized on a Keyence BIOREVO BZ-9000 microscope. The grade of defect healing was evaluated by three independent observers on three representative H&E stained sections per animal according to Huo *et al.* (26) using a scale ranging from fibrous tissue only (grade 0) to woven bone (grade 10).

SMA staining for visualization of blood vessels

Vascularization of the defect area was analyzed using a mouse anti-SMA antibody (dilution of 1:750; catalog no. M0851, Dako, Santa Clara, USA) following detection with the ImmPRESS-AP Anti-Mouse Immunoglobulin G Detection Kit (Vector Laboratories, Burlingame, USA) with Romulin (Biocare, Pacheco, USA) as chromogen. To ensure examination of the same area for all samples, the space between the inner holes of the screws was determined with a 2 \times objective. Using the software of the microscope (BZ-II Viewer), this area was separated in squares. In every square, the vessels present in the defect area were

counted using a 10× objective. Vessels of surrounding muscles or soft tissue were not included.

Serum assessment of TRAP5b

Blood was collected from all animals described in Table 1 at the time of euthanasia via the intracardiac route. Serum was separated from the whole blood by centrifugation (2000 rpm for 10 min) and frozen at -80°C until a day before the assay. All samples were allowed to thaw at 4°C overnight and diluted with saline by mixing 25 μl of the sample with 75 μl of normal saline on the day of the assay. After this, the manufacturer's assay guidelines (Immunodiagnostic Systems, document no. SB-TR102, version 08) were followed to perform the assay. All samples were analyzed in duplicate and averaged at the end to calculate the effective concentration of TRAP5b per sample. A set of four standard protein concentrations were used for plotting a standard curve, and a spiked rat serum sample containing known amount of TRAP5b was used for calculation of percent recovery. The standard and the spiked sample were provided by the manufacturer.

Animal ethics

The animal experiment was approved by the Local Animal Care Committee of Dresden University Hospital (protocol number: DD24-5131/354/10), and guidelines set by the National Institutes of Health for the use of experimental animals were followed.

Statistical methods

All data were tested for normality using the Shapiro-Wilk normality assessment test. Differences between multiple groups were tested using one-way analysis of variance (ANOVA) with Tukey's post hoc method in case of normally distributed data. Its nonparametric equivalent Kruskal-Wallis test with Dunn's multiple comparison method was chosen for data not following Gaussian distribution (micro-CT data). Two independent groups were tested using Student's *t* test with Welch's modification (three-point bending data). Paired data analysis was performed using paired samples *t* test. $P < 0.05$ was set as the limit for statistical differences. All data are expressed as means \pm SD. All statistical analyses were performed using GraphPad Prism [Prism 8 for macOS, v8.2.0 (272), GraphPad Software Inc., San Diego, USA].

SUPPLEMENTARY MATERIALS

Supplementary material for this article is available at <http://advances.sciencemag.org/cgi/content/full/6/48/eabc1779/DC1>

REFERENCES AND NOTES

- J. C. Reichert, S. Saifzadeh, M. E. Wullschleger, D. R. Epari, M. A. Schütz, G. N. Duda, H. Schell, M. van Griensven, H. Redl, D. W. Hutmacher, The challenge of establishing preclinical models for segmental bone defect research. *Biomaterials* **30**, 2149–2163 (2009).
- J. F. Keating, A. H. R. W. Simpson, C. M. Robinson, The management of fractures with bone loss. *J. Bone Joint Surg.* **87-B**, 142–150 (2005).
- T. T. Roberts, A. J. Rosenbaum, Bone grafts, bone substitutes and orthobiologics: The bridge between basic science and clinical advancements in fracture healing. *Organogenesis* **8**, 114–124 (2012).
- C. G. Finkemeier, Bone-grafting and bone-graft substitutes. *J. Bone Joint Surg. Am.* **84**, 454–464 (2002).
- P. Pelissier, A. C. Masquelet, R. Bareille, S. M. Pelissier, J. Amedee, Induced membranes secrete growth factors including vascular and osteoinductive factors and could stimulate bone regeneration. *J. Orthop. Res.* **22**, 73–79 (2004).
- U. K. Olesen, H. Eckardt, P. Bosemark, A. W. Paulsen, B. Dahl, A. Hede, The Masquelet technique of induced membrane for healing of bone defects. A review of 8 cases. *Injury* **46**, S44–S47 (2015).
- M. M. Stevens, Biomaterials for bone tissue engineering. *Mater. Today* **11**, 18–25 (2008).
- M. Rodríguez-Évora, A. Delgado, R. Reyes, A. Hernández-Daranas, I. Soriano, J. S. Román, C. Évora, Osteogenic effect of local, long versus short term BMP-2 delivery from a novel SPU–PLGA– β TCP concentric system in a critical size defect in rats. *Eur. J. Pharm. Sci.* **49**, 873–884 (2013).
- H. Uludag, D. D'Augusta, R. Palmer, G. Timony, J. Wozney, Characterization of rhBMP-2 pharmacokinetics implanted with biomaterial carriers in the rat ectopic model. *J. Biomed. Mater. Res.* **46**, 193–202 (1999).
- A. W. James, G. L. Chaud, J. Shen, G. Asatrian, V. Nguyen, X. Zhang, K. Ting, C. Soo, A review of the clinical side effects of bone morphogenetic protein-2. *Tissue Eng. Part B Rev.* **22**, 284–297 (2016).
- N. Mathavan, P. Bosemark, H. Isaksson, M. Tägil, Investigating the synergistic efficacy of BMP-7 and zoledronate on bone allografts using an open rat osteotomy model. *Bone* **56**, 440–448 (2013).
- D. G. Little, M. McDonald, R. Bransford, C. B. Godfrey, N. Amanat, Manipulation of the anabolic and catabolic responses with OP-1 and zoledronic acid in a rat critical defect model. *J. Bone Miner. Res.* **20**, 2044–2052 (2005).
- D. B. Raina, H. Isaksson, W. Hettwer, A. Kumar, L. Lidgren, M. Tägil, A biphasic calcium sulphate/hydroxyapatite carrier containing bone morphogenetic protein-2 and zoledronic acid generates bone. *Sci. Rep.* **6**, 26033 (2016).
- M. T. Drake, B. L. Clarke, S. Khosla, Bisphosphonates: Mechanism of action and role in clinical practice. *Mayo Clin. Proc.* **83**, 1032–1045 (2008).
- D. B. Raina, D. Larsson, F. Mrkonjic, H. Isaksson, A. Kumar, L. Lidgren, M. Tägil, Gelatin-hydroxyapatite-calcium sulphate based biomaterial for long term sustained delivery of bone morphogenetic protein-2 and zoledronic acid for increased bone formation: In-vitro and in-vivo carrier properties. *J. Control. Release* **272**, 83–96 (2018).
- D. B. Raina, D. Larsson, E. A. Sezgin, H. Isaksson, M. Tägil, L. Lidgren, Biomodulation of an implant for enhanced bone-implant anchorage. *Acta Biomater.* **96**, 619–630 (2019).
- A. Abramo, M. Geijer, P. Kopylov, M. Tägil, Osteotomy of distal radius fracture malunion using a fast remodeling bone substitute consisting of calcium sulphate and calcium phosphate. *J. Biomed. Mater. Res. B Appl. Biomater.* **92B**, 281–286 (2010).
- A. Abramo, M. Tägil, M. Geijer, P. Kopylov, Osteotomy of dorsally displaced malunited fractures of the distal radius: No loss of radiographic correction during healing with a minimally invasive fixation technique and an injectable bone substitute. *Acta Orthop.* **79**, 262–268 (2008).
- P. F. Horstmann, W. H. Hettwer, N. S. Kalsoft, M. M. Petersen, Early clinical and radiological experience with a ceramic bone graft substitute in the treatment of benign and borderline bone lesions. *Sci. Rep.* **8**, 15384 (2018).
- M. A. McNally, J. Y. Ferguson, A. C. K. Lau, M. Diefenbeck, M. Scarborough, A. J. Ramsden, B. L. Atkins, Single-stage treatment of chronic osteomyelitis with a new absorbable, gentamicin-loaded, calcium sulphate/hydroxyapatite biocomposite. *Bone Jt. J.* **98-B**, 1289–1296 (2016).
- P. F. Horstmann, D. B. Raina, H. Isaksson, W. Hettwer, L. Lidgren, M. M. Petersen, M. Tägil, Composite biomaterial as a carrier for bone-active substances for metaphyseal tibial bone defect reconstruction in rats. *Tissue Eng. Part A* **23**, 1403–1412 (2017).
- X. Dong, Q. Wang, T. Wu, H. Pan, Understanding adsorption-desorption dynamics of BMP-2 on hydroxyapatite (001) surface. *Biophys. J.* **93**, 750–759 (2007).
- G. H. Nancollas, R. Tang, R. J. Phipps, Z. Henneman, S. Gulde, W. Wu, A. Mangood, R. G. G. Russell, F. H. Ebetino, Novel insights into actions of bisphosphonates on bone: Differences in interactions with hydroxyapatite. *Bone* **38**, 617–627 (2006).
- E. Segredo-Morales, P. García-García, C. Évora, A. Delgado, BMP delivery systems for bone regeneration: Healthy vs osteoporotic population. *Review. J. Drug Deliv. Sci. Technol.* **42**, 107–118 (2017).
- J.-S. Wang, M. Tägil, H. Isaksson, M. Boström, L. Lidgren, Tissue reaction and material biodegradation of a calcium sulfate/apatite biphasic bone substitute in rat muscle. *J. Orthop. Translat.* **6**, 10–17 (2016).
- M. H. Huo, N. W. Troiano, R. R. Pelker, C. M. Gundersen, G. E. Friedlaender, The influence of ibuprofen on fracture repair: Biomechanical, biochemical, histologic, and histomorphometric parameters in rats. *J. Orthop. Res.* **9**, 383–390 (1991).
- M. R. Urist, Bone: Formation by autoinduction. *Science* **150**, 893–899 (1965).
- D. B. Raina, H. Isaksson, A. K. Teotia, L. Lidgren, M. Tägil, A. Kumar, Biocomposite macroporous cryogels as potential carrier scaffolds for bone active agents augmenting bone regeneration. *J. Control. Release* **235**, 365–378 (2016).
- C. M. Murphy, A. Schindeler, J. P. Gleeson, N. Y. C. Yu, L. C. Cantrill, K. Mikulec, L. Peacock, F. J. O'Brien, D. G. Little, A collagen-hydroxyapatite scaffold allows for binding and co-delivery of recombinant bone morphogenetic proteins and bisphosphonates. *Acta Biomater.* **10**, 2250–2258 (2014).
- K. Sato, Y. Watanabe, N. Harada, S. Abe, T. Matsushita, K. Yamanaka, T. Kaneko, Y. Sakai, Establishment of reproducible, critical-sized, femoral segmental bone defects in rats. *Tissue Eng. Part C Methods* **20**, 1037–1041 (2014).

31. M. H. Hettiaratchi, L. Krishnan, T. Rouse, C. Chou, T. C. McDevitt, R. E. Guldberg, Heparin-mediated delivery of bone morphogenetic protein-2 improves spatial localization of bone regeneration. *Sci. Adv.* **6**, eaay1240 (2020).
32. B. Zhang, J. D. Skelly, J. R. Maalouf, D. C. Ayers, J. Song, Multifunctional scaffolds for facile implantation, spontaneous fixation, and accelerated long bone regeneration in rodents. *Sci. Transl. Med.* **11**, eaau7411 (2019).
33. W. F. McKay, S. M. Peckham, J. M. Badura, A comprehensive clinical review of recombinant human bone morphogenetic protein-2 (INFUSE[®] Bone Graft). *Int. Orthop.* **31**, 729–734 (2007).
34. J. N. Zara, R. K. Siu, X. Zhang, J. Shen, R. Ngo, M. Lee, W. Li, M. Chiang, J. Chung, J. Kwak, B. M. Wu, K. Ting, C. Soo, High doses of bone morphogenetic protein 2 induce structurally abnormal bone and inflammation in vivo. *Tissue Eng. Part A* **17**, 1389–1399 (2011).
35. L. Krishnan, L. B. Priddy, C. Esancy, B. S. Klosterhoff, H. Y. Stevens, L. Tran, R. E. Guldberg, Delivery vehicle effects on bone regeneration and heterotopic ossification induced by high dose BMP-2. *Acta Biomater.* **49**, 101–112 (2017).
36. S. S. Lee, B. J. Huang, S. R. Kaltz, S. Sur, C. J. Newcomb, S. R. Stock, R. N. Shah, S. I. Stupp, Bone regeneration with low dose BMP-2 amplified by biomimetic supramolecular nanofibers within collagen scaffolds. *Biomaterials* **34**, 452–459 (2013).
37. P. Bosemark, H. Isaksson, M. Tägil, Influence of systemic bisphosphonate treatment on mechanical properties of BMP-induced calluses in a rat fracture model: Comparison of three-point bending and twisting test. *J. Orthop. Res.* **32**, 721–726 (2014).
38. T. Morimoto, T. Kaito, Y. Matsuo, T. Sugiura, M. Kashii, T. Makino, M. Iwasaki, H. Yoshikawa, The bone morphogenetic protein-2/7 heterodimer is a stronger inducer of bone regeneration than the individual homodimers in a rat spinal fusion model. *Spine J.* **15**, 1379–1390 (2015).
39. A. A. Lloyd, B. Gludovatz, C. Riedel, E. A. Luengo, R. Saiyed, E. Marty, D. G. Lorch, J. M. Lane, R. O. Ritchie, B. Busse, E. Donnelly, Atypical fracture with long-term bisphosphonate therapy is associated with altered cortical composition and reduced fracture resistance. *Proc. Natl. Acad. Sci. U.S.A.* **114**, 8722–8727 (2017).
40. D. M. Black, P. D. Delmas, R. Eastell, I. R. Reid, S. Boonen, J. A. Cauley, F. Cosman, P. Lakatos, P. C. Leung, Z. Man, C. Mautalen, P. Mesenbrink, H. Hu, J. Caminis, K. Tong, T. Rosario-Jansen, J. Krasnow, T. F. Hue, D. Sellmeyer, E. F. Eriksen, S. R. Cummings; HORIZON Pivotal Fracture Trial, Once-yearly zoledronic acid for treatment of postmenopausal osteoporosis. *N. Engl. J. Med.* **356**, 1809–1822 (2007).
41. I. Lambrinoudaki, S. Vlachou, F. Galapi, D. Papadimitriou, K. Papadias, Once-yearly zoledronic acid in the prevention of osteoporotic bone fractures in postmenopausal women. *Clin. Interv. Aging* **3**, 445–451 (2008).
42. D. B. Raina, I. Qayoom, D. Larsson, M. H. Zheng, A. Kumar, H. Isaksson, L. Lidgren, M. Tägil, Guided tissue engineering for healing of cancellous and cortical bone using a combination of biomaterial based scaffolding and local bone active molecule delivery. *Biomaterials* **188**, 38–49 (2019).
43. S. J. Sample, R. J. Collins, A. P. Wilson, M. A. Racette, M. Behan, M. D. Markel, V. L. Kalscheur, Z. Hao, P. Muir, Systemic effects of ulna loading in male rats during functional adaptation. *J. Bone Miner. Res.* **25**, 2016–2028 (2010).

Acknowledgments: We thank T. von Strauwitz for producing the 3D printed saw guides and A. Wenke and S. Manthey for preparing the histological sections. **Funding:** We are grateful for the infrastructure support provided by the University Hospital Carl Gustav Carus at Technische Universität Dresden, Center for Translational Bone, Joint, and Soft Tissue Research and University Center of Orthopaedics and Traumatology, Dresden, Germany and the Medical Faculty, Lund University Sweden. VINNOVA, the Swedish Agency for Innovation Systems (grant no. 2017-00269) is thanked for partly covering the financial expenses. **Author contributions:** S.Z., M.T., D.B.R., C.V., J.B., and H.I.: study conception and planning. L.L., D.B.R., M.T., and L.-M.M.: CaS/HA biomaterial preparation. S.Z., C.V., L.-M.M., J.B., and D.B.R.: animal surgery and care, injections, and blood collection. L.M.M., C.V., D.B.R., H.I., and S.Z.: analysis of defect healing. D.B.R. and L.M.M.: data collection and analysis with input from H.I., S.Z., and C.V. D.B.R.: wrote the first draft of the manuscript. All authors: manuscript revision. **Competing interests:** L.L. is a board member of Ortho Cell, Australia and BONESUPPORT AB, Sweden. L.L. invented the CaS/HA biomaterial described in this study in his laboratory and holds a granted patent for the said biomaterial. M.T. and D.B.R. have received options from Orthocell Australia. The authors declare that they have no other competing interests pertaining to this study. **Data and materials availability:** All data related to this paper is provided in the main manuscript or the Supplementary Materials. Raw data can be made available upon a reasonable request to the senior author or the corresponding author of this study. Additional data related to this paper may be requested from the authors.

Submitted 9 April 2020

Accepted 9 October 2020

Published 27 November 2020

10.1126/sciadv.abc1779

Citation: D. B. Raina, L.-M. Matuszewski, C. Vater, J. Bolte, H. Isaksson, L. Lidgren, M. Tägil, S. Zwingenberger, A facile one-stage treatment of critical bone defects using a calcium sulfate/hydroxyapatite biomaterial providing spatiotemporal delivery of bone morphogenetic protein-2 and zoledronic acid. *Sci. Adv.* **6**, eabc1779 (2020).